INTERNATIONAL JOURNAL FOR NUMERICAL METHODS IN FLUIDS, VOL. 15, 251–271 (1992)

NUMERICAL MODELLING OF CAVITIES ON AXISYMMETRIC BODIES AT ZERO AND NON-ZERO ANGLE OF ATTACK

MARC S. INGBER

Department of Mechanical Engineering, University of New Mexico, Albuquerque, NM 87131, U.S.A.

AND

CHRIS E. HAILEY

Aerodynamics Department, Sandia National Laboratories, Albuquerque, NM 87185, U.S.A.

SUMMARY

The flow about submerged, fully cavitating axisymmetric bodies at both zero and non-zero angle of attack is considered in this paper. A cavity closure model that relates the point of detachment, the angle that the separating streamline makes with the body and the cavity length is described. The direct boundary element method is used to solve the potential flow problem and to determine the cavity shape. A momentum integral boundary layer solver is included in the formulation so that shear stresses can be incorporated into the drag calculations. The numerical predictions based on the proposed closure model are compared with water tunnel measurements and photographs.

KEY WORDS Cavitation flow Cavity closure model Drag on cavitating bodies Boundary element method

INTRODUCTION

The flow field about a submerged, fully cavitating three-dimensional body poses several difficult problems for the analyst. These problems include determining the point at which the dividing streamline which defines the cavity detaches from the body, the angle at which the dividing streamline leaves the body, the shape of the cavity and the length of the cavity. By fully cavitating flows (following Plesset[1] and Arakeri[2]) we mean that the flow is characterized by a single large vapour cavity enveloping some portion of the body. If the cavity extends past the end of the body, the body is said to be supercavitating. If the cavity reattaches on the body, the body is said to be partially cavitating. The problems associated with modelling flows about partially or supercavitating bodies are not easy to resolve because of the complex way that cavitation depends on the body geometry and the state of flow. The shape and extent of the cavity will have a significant effect on the resultant forces and moments acting on the body. Hence timely and inexpensive estimates of cavity shapes are desirable.

There is presently no unified theory for modelling cavitating flows over bodies because of the complexities of the flow field and the lack of adequate experimental data. This necessitates the development of closure models to allow for the prediction of cavity shapes. Several closure models have previously been proposed for approximating the shape of the aft portion of the

0271–2091/92/150251–21$15.50

Received 19 March 1991
Revised 25 November 1991

cavity, the location of the point of detachment and the angle at which the dividing streamline leaves the body. Apparently, however, no closure model has been proposed for determining the cavity length. This is surprising, because none of these closure problems is independent. In this paper we propose a method of determining the cavity shape and length based on the relationship between the point of detachment, the angle at which the dividing streamline leaves the body and the cavity length.

Perhaps the most widely discussed closure problem is that of determining the shape of the aft portion of the cavity in the region of turbulent two-phase flow. One of the oldest closure models (and perhaps still the most widely used) was formulated by Riabouchinski.[3] This model assumes longitudinal symmetry through the plane of maximum thickness of the cavity. However, a wide variety of competing closure models have been formulated, including the open wake model,[4,5] the re-entrant jet model,[6] the vortex model[7] and the displacement thickness model.[8]

Two closure problems which are generally considered together are those of determining the location of the point of detachment and the angle at which the dividing streamline separates from the body. In some cases, such as for bodies with discontinuous slopes, the point of detachment and the angle at which the dividing streamline leaves the body are easy to determine. In these situations the cavity detaches at the body juncture parallel to the attached flow.[2] However, if the body geometry is smooth, these problems are more difficult to resolve. From pure potential theory the curvature of the dividing streamline at the point of detachment must be finite, or equivalently, the dividing streamline must be parallel to the body at the point of detachment. This condition was first proposed by Brillouin[9] and Villat[10] and is designated as the smooth separation condition. The rationale for this condition is that it is impossible under the assumption of potential flow to maintain the cavitation pressure at a cusp in the geometry. Further, assuming the smooth detachment condition and remaining within the framework of potential theory, the point of detachment is located at the body station where the pressure first drops below the cavitation pressure. However, the experimental evidence often contradicts the smooth separation condition.

There are essentially two different types of cavitation separation, which Arakeri[2] designates as nucleate and viscous laminar. For nucleate separation the smooth separation condition provides a reasonable closure model. However, for viscous laminar separation the experimentally determined position of cavitation separation lies considerably downstream from that predicted by the smooth separation condition.[2,11] Viscous laminar separation is observed on bodies which possess a laminar boundary layer separation under non-cavitating conditions. Further, from photographs of this type of cavitation it appears that the dividing streamline defining the cavity leaves the body at an oblique angle. Arakeri[2] developed a semi-empirical method to predict the position of the point of detachment for viscous laminar separation on smooth bodies.

Numerical methods to predict cavity shapes on two-dimensional and axisymmetric bodies have been developed by Brennen,[11] Mogel and Street,[12] Furuya,[13] Pellone and Rowe,[14] Dagan,[15] Aitchison and Karageorghis,[16] Lemonnier and Rowe[8] and others. These researchers have used many of the closure models discussed above in their algorithms. However, common to all their methods, the cavity length has been assumed to be known *a priori*. In practice the cavity length is not known *a priori* and therefore some method is necessary in order to predict this length. In this paper we formulate a closure model to predict the cavity length. We are using the term closure model here in a somewhat wider context than in the literature, in that the closure model is used not only to approximate the shape of the aft portion of the cavity but also to determine the point of detachment, the angle that the dividing streamline makes with the attached flow and the cavity length. In order to validate the proposed closure model, we compare the results based on the model with a wide variety of water tunnel data.

The closure model to predict the cavity length is based on the relationship between the point of detachment, the angle at which the dividing streamline leaves the body and the cavity length. We assume for our closure model that the point of detachment and the angle that the dividing streamline makes with the body are known. In particular, we limit our attention in this paper to fully cavitating flows about bodies without laminar separation bubbles, for which the smooth separation condition is valid. Given the point of detachment as determined from the smooth separation condition and an assumed cavity length, we employ the direct boundary element method (DBEM) to determine the shape of a constant pressure streamline representing the cavity, which we will call the dividing streamline. This is readily accomplished by the DBEM except at the leading and trailing edges of the dividing streamline. The resulting shape of the dividing streamline can be quite different than the cavity formation observed in the water tunnel. The reason for this is due, for the most part, to the fact that the pressure at the leading edge of the dividing streamline is not equal to the cavitation pressure. This in turn is a consequence of the fact that the angle that the dividing streamline makes with the body does not satisfy the smooth separation condition. Hence the criterion for whether the dividing streamline will accurately approximate the shape of the cavity surface is based on whether the angle at which the dividing streamline leaves the body satisfies the smooth separation condition. If the angle is incorrect, then the assumed cavity length must be adjusted until the angle matches the prescribed angle. Only when the smooth separation condition is satisfied will the condition of constant pressure extend to the leading edge of the dividing streamline. We discuss the mechanics of adjusting the cavity length in order to achieve the proper angle that the dividing streamline makes with the body at the point of detachment.

In the following sections we apply our closure model to a wide variety of body geometries and flow conditions. We consider both axisymmetric flows and flows at an angle of attack. After considering several purely potential solutions, we incorporate a momentum integral boundary layer solution into our numerical formulation in order to more accurately calculate the drag force exerted on cavitating bodies. In these calculations we show that it is important to be able to accurately predict the cavity length.

PROBLEM FORMULATION AND NUMERICAL PROCEDURE

The governing equation, assuming incompressible, irrotational and inviscid flow, in terms of the potential function ϕ is given by Laplace's equation. The potential function can be subdivided into two parts: one part due to the free stream, ϕ_{fs}, and the other part due to the perturbation caused by the body and cavity, ϕ_p. A typical problem geometry is shown in Figure 1. Initially we must assume a position for the cavity. Let Γ_1 represent the wetted portion of the body and Γ_2 represent the surface of the cavity. Then the differential system can be written as

$$\nabla^2\phi = \nabla^2\phi_{fs} + \nabla^2\phi_p = 0, \tag{1}$$

$$\frac{\partial\phi_{fs}}{\partial n} = -\frac{\partial\phi_p}{\partial n} \quad \text{on } \Gamma_1 \text{ and } \Gamma_2, \tag{2}$$

$$\left(\frac{\partial\phi}{\partial x}\right)^2 + \left(\frac{\partial\phi}{\partial y}\right)^2 = C^2 \quad \text{on } \Gamma_2, \tag{3}$$

where ∇^2 is the three-dimensional Laplacian operator, $\partial/\partial n$ is the derivative in the direction of the outward normal to the surface and C is a constant representing the liquid velocity along the

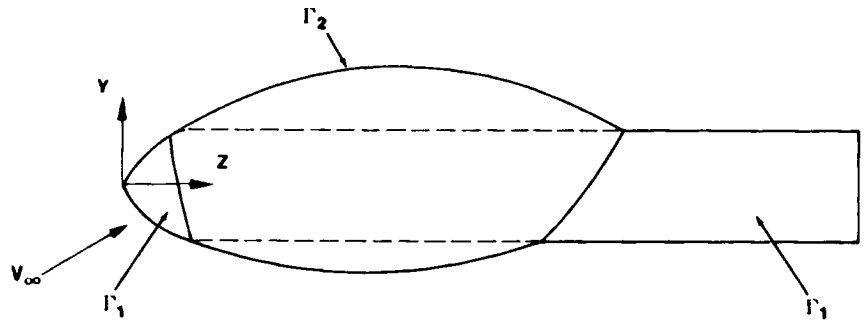

Figure 1. Typical problem geometry

cavity surface. This constant is related to the cavitation number K through the equation

$$K = \frac{P_\infty - P_c}{\rho V_\infty^2/2} = C^2 - 1, \tag{4}$$

where P_∞ is the free stream pressure, P_c is the pressure inside the cavity,* ρ is the liquid density and V_∞ is the free stream velocity. This problem is highly non-linear, not only because (3) represents a non-linear boundary condition but also because the position of the boundary Γ_2 is unknown *a priori*. Nevertheless, assuming the point of detachment and the cavity length, a solution can be found to the differential system discussed above except at the leading and trailing edges of the cavity, the so-called detachment and reattachment zones.

We use a displacement thickness model to connect the cavity to the body in the reattachment zone. The displacement thickness model was selected after performing several numerical experiments. If the boundary element node just upstream of the reattachment node is a midside node, the displacement thickness is chosen as 75% of the cavity thickness at the next upstream node under the cavity. If the boundary element node just upstream of the reattachment node is an edge node, the displacement thickness is chosen as 25% of the cavity thickness at the next upstream node under the cavity. The actual values chosen for the displacement thicknesses were selected because they improved the overall convergence of the numerical algorithm without having much influence on the upstream shape of the cavity. Using the displacement thickness model, the calculated pressure at the last two nodes under the cavity may not be equal to the cavitation pressure. Nevertheless, the flow is two-phase, bubbly and turbulent in this region, thus making a cavity termination model necessary.

The solution determined using the displacement thickness model may still not approximate the physical cavity because of the selection of an improper point of detachment and improper cavity length. In the present paper we will assume that we can correctly predict the point of detachment and focus on determining the correct cavity length. This is accomplished by an inner and outer

* In this paper we have chosen to define the cavitation number using the measured cavity pressure rather than the vapour pressure. This definition is consistent with most experiments cited in this work, e.g. those of Stinebring *et al.*[17] and O'Neill[18], where actual cavity pressures were measured. However, there are several experiments cited in this work where the cavitation number is defined in terms of the vapour pressure. Rouse and McNown[19] have shown that in experiments with blunt headforms, where boundary layer separation has occurred, the pressure in the cavity is greater than the vapour pressure. However, for slender headforms the experimental results indicate that the cavity pressure is very close to the vapour pressure for a wide range of cavitation numbers. Since the experimental results cited in this paper are for fairly slender headforms without laminar separation, we will use a single definition for the cavitation number and not distinguish between measured cavity pressure and assumed vapour cavity pressure.

iteration. In the inner iteration a constant pressure streamline is determined for the assumed cavity length using a Newton–Raphson iteration. In the outer iteration the cavity length is adjusted until our closure condition is satisfied.

The inner iteration

Given a point of detachment and cavity length, an initial cavity shape must be assumed. The initial estimate of the cavity shape can have a large influence on the convergence rate and subsequent cost of the method. We discuss in the results how this initial estimate is made for several body geometries. We employ the direct boundary element method (DBEM) in our calculations. Following standard formulation procedures for the DBEM (see e.g. Reference 20), ϕ_p may be represented in terms of a boundary integral as

$$\eta(\xi)\phi_p(\xi) = \int_\Gamma \left(\frac{\partial G(\xi, \mathbf{x})}{\partial n(\mathbf{x})} \phi_p(\mathbf{x}) - G(\xi, \mathbf{x}) \frac{\partial \phi_p(\mathbf{x})}{\partial n(\mathbf{x})} \right) d\Gamma(\mathbf{x}), \tag{5}$$

where $\Gamma = \Gamma_1 + \Gamma_2$ represents the wetted portion of the body and the cavity surface. The free space Green function $G(\xi, \mathbf{x})$ is given by

$$G(\xi, \mathbf{x}) = \frac{1}{|\xi - \mathbf{x}|}. \tag{6}$$

The coefficient $\eta(\xi)$ can be calculated from (5) by assuming a constant source strength ϕ_p along the surface and hence is given by

$$\eta(\xi) = \int_\Gamma \frac{\partial G(\xi, \mathbf{x})}{\partial n(\mathbf{x})} d\Gamma(\mathbf{x}). \tag{7}$$

The integral equation (5) is discretized by approximating the boundary Γ with isoparametric boundary elements. The element library used in this research consists of the six-node triangular element and the nine-node quadrilateral element. Double nodes are placed along all geometric edges to resolve the ambiguity in the normal direction and enhance the accuracy of the solution.[21] Collocating (5) at each of the N nodes within the boundary elements leads to the system of N equations given symbolically by

$$[G_{ij}]\{\phi_j\} = [H_{ij}]\{\phi'_j\}, \tag{8}$$

where ϕ_j and ϕ'_j represent the values of the perturbed potential function and its normal derivative respectively at the collocation nodes within the boundary elements. In traditional boundary element methods, either the perturbed potential ϕ_p, the flux ϕ'_p or a linear combination of the two is specified at each collocation node and (8) is rearranged (assembled) in order to solve for the remaining unknowns. In the present analysis, only one of the two boundary conditions, (2) or (3), can be prescribed along the cavity surface Γ_2. In general, if the kinematic condition (2) is prescribed, then the dynamic condition (3) will not be satisfied, and vice versa.

We consider a parametrization of the cavity. For axisymmetric bodies at 0° angle of attack, this parametrization can be represented in terms of the radii r_i at body stations z_i. An alternative representation is in terms of the coefficients a_i of the truncated Fourier sine series

$$r(z) = \sum_{n=1}^{m} a_n \sin(n\pi z), \tag{9}$$

where r represents the radius at the body station z. For an axisymmetric body at an angle of attack we can represent the cavity in terms of the radii r_{ij} at body stations z_i and the polar angle

θ_j. As a generalization we consider the cavity to be parametrized by the coefficients $c_1, c_2, \ldots, c_m$. We impose the no-penetration condition (2) at the boundary element nodes on the surface of the cavity. As mentioned above, upon solution of the discretized boundary element equations, the condition of constant velocity along the surface of the cavity (3) will not be satisfied. However, these velocities will be functions of the coefficients c_i. Therefore the condition of constant velocity at the nodes on the surface of the cavity can be written in symbolic form as

$$\mathbf{F}(c_1, c_2, \ldots, c_m) = 0. \tag{10}$$

The non-linear implicit vector equations represented by (10) are solved by iteration using a Newton–Raphson scheme. Since the explicit form of $\mathbf{F}$ is unknown, the partial derivatives $\partial\mathbf{F}/\partial c_i$ contained in the Jacobian matrix are determined by perturbing the coefficients c_i individually, determining the potential solution on the perturbed cavity shape and using a finite difference approximation for the partial derivatives. Typically, converged shapes could be determined within five iterations. However, since the cavity thickness at the leading edge is prescribed to be zero, it is not a parameter of the cavity modelling and hence the dynamic boundary condition at the leading edge of the cavity cannot be satisfied in the inner iteration. Thus an outer iteration in which the cavity length is adjusted is necessary in order to satisfy the dynamic boundary condition at the cavity leading edge.

The outer iteration

Although a solution for the shape of the cavity with the assumed point of detachment and length satisfying (1)–(3) can be generated, it may be physically unrealistic in that it may be too thick or too thin. We propose the following closure model. As mentioned previously, we assume that the point of detachment and the angle at which the dividing streamline leaves the body are known. There is a relationship between the assumed cavity length, the cavity thickness and the angle at which the cavity leaves the body. We use the term cavity in a loose sense here, in that the shapes generated in the inner iteration do not satisfy the dynamic boundary condition at the leading edge of the cavity. From numerical experiment it was determined that as the assumed cavity length is increased, the cavity becomes thicker and the angle at which the cavity leaves the body increases. Hence in the outer iteration, if the angle at which the cavity leaves the body calculated in the previous iteration is too small, the assumed cavity length is increased. Similarly, if the angle is too large, the assumed cavity length is decreased. The length is adjusted until the dividing streamline leaves the body at the prescribed angle. This iteration then determines the unique cavity length for which the dynamic boundary condition is satisfied everywhere along the cavity surface except at the last two boundary element nodes where the displacement thickness model is applied. Although it is possible to perform the outer iteration using a Newton–Raphson method, it proved more economical to use educated trial and error to adjust the cavity length.

RESULTS FOR AXISYMMETRIC FLOWS

We first consider a 1 calibre ogive cylinder with the cavitation number given by $K = 0{\cdot}24$. The length of the body is 4·866 calibre. Since this body is relatively slender, we do not expect a laminar separation. Hence we assume the smooth separation condition. On this basis the leading edge of the cavity is set at $z = 0{\cdot}366\,03$ calibre, since this is where the pressure drops below the cavitation pressure on the fully wetted body. The results of the inner iteration for three assumed cavity lengths are shown in Figure 2. The cavity shape in Figure 2(a) is seen to penetrate into the ogive surface, which is physically impossible. The cavity shape in Figure 2(b) is seen to be essentially

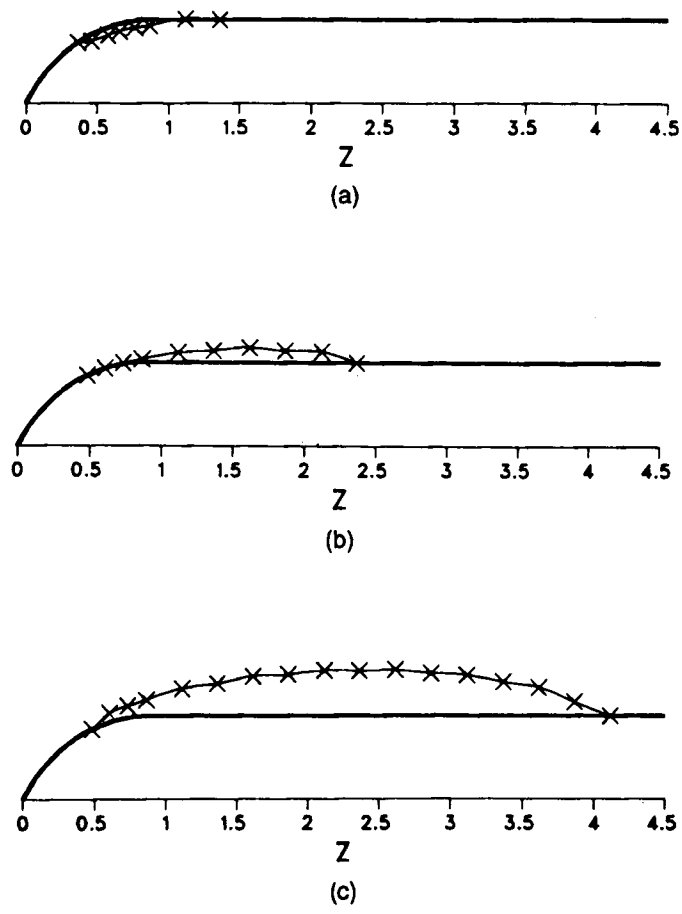

Figure 2. Calculated cavity shapes for 1 calibre ogive body with cavitation number $K = 0{\cdot}24$: (a) cavity length $L = 1{\cdot}1$, (b) $L = 2{\cdot}2$, (c) $L = 3{\cdot}8$

tangent to the ogive surface at its leading edge. The cavity shape in Figure 2(c) is seen to leave the ogive surface at an oblique angle. Using the closure model discussed in the previous section consistent with the smooth separation condition, the cavity shape shown in Figure 2(b) is chosen as the one best representing the actual physical cavity. The cavity is compared with the water tunnel photographs and measurements of Rouse and McNown[19] in Figure 3. The comparison of the measured and computed cavity shapes is quite good over the entire length of the cavity. The measured and computed pressure distributions also compare quite well except near the point of reattachment. However, as was already mentioned, the modelling of the aft portion of the cavity is deficient because the flow is non-steady and turbulent in this region and this is where the displacement thickness model is imposed.

We next consider a body comprised of a 45° conical head and a cylindrical midbody with the cavitation number given by $K = 0{\cdot}30$. The length of the body is 5·207 calibre. For this body with the abrupt change in normal direction at the juncture between the conical nose and the cylindrical midbody, the cavity detachment is at the body juncture and the cavity must leave the body at a 22·5° angle. We show similar results in Figures 4 and 5 as were shown for the ogive body in

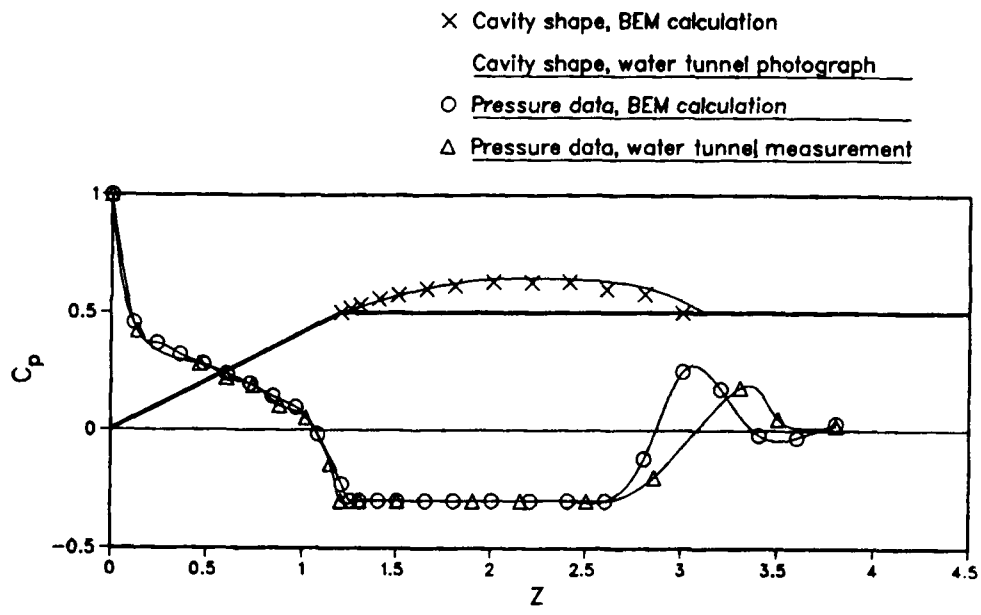

Figure 3. Comparison of DBEM and water tunnel results for 1 calibre ogive body with cavitation number $K = 0{\cdot}24$

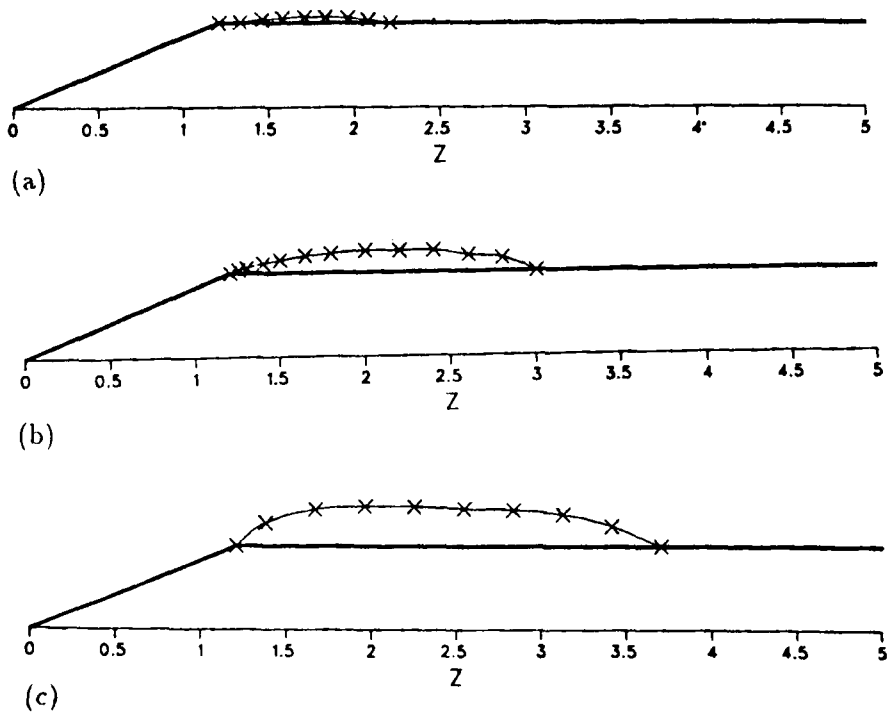

Figure 4. Calculated cavity shapes for 45° cone–cylinder body with cavitation numbers $K = 0{\cdot}3$: (a) cavity length $L = 1{\cdot}0$, (b) $L = 1{\cdot}8$, (c) $L = 2{\cdot}6$

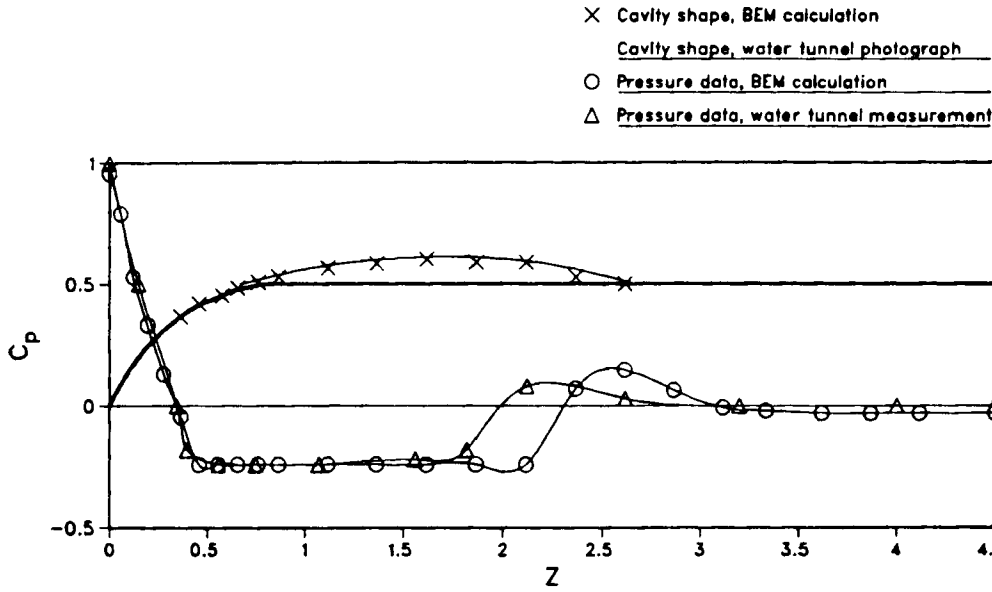

Figure 5. Comparison of DBEM and water tunnel results for 45° cone–cylinder body with cavitation number $K = 0{\cdot}3$

Figures 2 and 3. The cavity shape in Figure 4(b) is seen to possess the proper angle at the leading edge and hence is chosen as the one best representing the actual physical cavity. This cavity is compared with the water tunnel photographs and measurements of Rouse and McNown[19] in Figure 5. Again the comparisons are quite good.

As discussed in the previous section, there are two iterations being performed to determine the cavity shape. In the inner iteration the cavity length is assumed and a Newton–Raphson iteration is performed to determine the location of the constant pressure streamline. The rate of convergence of the inner iteration is dependent on the initial estimate for the location of the dividing streamline. In fact, if the initial estimate is poor, the iteration may not converge at all. It is therefore beneficial to have a method for generating initial estimates of the cavity shape capable of reducing the computational costs. Following Wolfe *et al.*,[22] the initial estimates for the ogive bodies are generated by assuming the point of detachment and the cavity length and then fitting an arc of a circle through these points which is tangent to the body at the point of detachment. The convergence of the Newton–Raphson iteration with this initial cavity shape is demonstrated in Figure 6 for the cavity on the 1 calibre ogive body shown in Figure 2(b). In general, we could achieve pressures at the nodes of the boundary elements comprising the cavity that were within 0·1% of the cavitation pressure within five iterations.

A comparison of the DBEM results generated using the current closure model (assuming the smooth separation condition) with the water tunnel results of Rouse and McNown[19] for a variety of headforms with cylindrical midbodies is shown in Table I. The DBEM results are seen to be in good agreement with the water tunnel results except possibly for the hemispherical head at a cavitation number $K = 0{\cdot}24$. In this case the predicted cavity length is 14% too short. It is possible, however, that for this relatively blunt body a small laminar separation bubble exists and hence the smooth separation condition would no longer apply.

We next consider in more detail the body comprised of a 45° conical nose and a cylindrical midbody. For this body the point of detachment is at the body juncture and the angle of the cavity

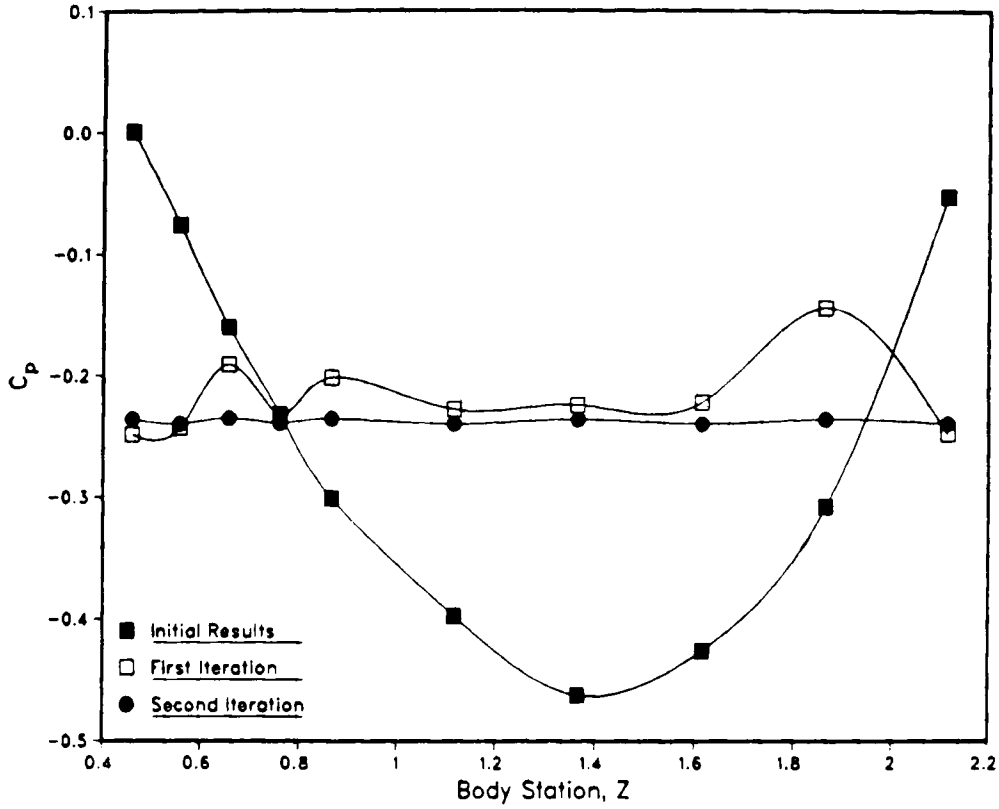

Figure 6. Coefficient-of-pressure calculations for assumed initial cavity shape and cavity shapes determined from first two Newton–Raphson iterations

Table I. Comparisons between DBEM results and water tunnel results for limited cavitation on axisymmetric bodies

Headform	Cavitation number	Cavity length		Maximum thickness	
		DBEM	Experiment	DBEM	Experiment
Ogive (0·25 calibre)	0·5	1·4	1·3	0·15	0·15
Hemispherical	0·24	3·3	3·8	0·20	0·25
Hemispherical	0·32	1·9	1·7	0·12	0·11
Hemispherical	0·40	1·2	1·2	0·08	0·07
Ogive (1 calibre)	0·24	2·0	2·1	0·10	0·09
Ogive (1 calibre)	0·32	0·75	0·74*†	0·05	—†
Ogive (1 calibre)	0·40	0·66	0·64*†	0·04	—†
Ogive (2 calibre)	0·20	1·7	1·8	0·06	0·08
Conical (45°)	0·3	1·8	1·8	0·12	0·13
Conical (45°)	0·5	0·82	0·83	0·07	0·08
Conical (90°)	0·5	1·70	1·60	0·23	0·22

* The cavity length was estimated from the pressure data provided by Rouse and McNown.[19]
† The cavity thickness and length were not discernible form the water tunnel photographs.

at the point of detachment is parallel to the attached flow. Stinebring *et al.*[17] performed a series of water tunnel experiments to determine the relationship between the cavity length and the cavitation number for this body. Self and Ripken[23] performed a similar set of experiments on a 45° supercavitating conical body with no afterbody. Self and Ripken considered vapour cavities while Stinebring *et al.* considered ventilated cavities. In addition, Self and Ripken measure the maximum cavity diameter. Semi-empirical expressions for the cavity length and maximum cavity diameter on supercavitating conical bodies were determined by Reichardt.[24] We compare the present DBEM results for the cavity length with these sets of results in Figure 7. The DBEM results match the two sets of experimental results and Reichardt's semi-empirical formula very well for small cavitation numbers. As the cavitation number increases, the various sets of results diverge somewhat but are still fairly consistent. There are several factors which could contribute to the discrepancies in the results for the larger cavitation numbers. At these larger cavitation numbers the cavities are relatively short. The effects of the afterbody (compared to cones without afterbodies), the differences between vapour cavities and ventilated cavities and the difficulties in determining the cavity lengths from photographs could be more pronounced for shorter cavities. Nevertheless, the DBEM results compare favourably with the data, further demonstrating the validity of the closure model. The relationship between the maximum cavity thickness and the cavitation number is shown in Figure 8. Again the DBEM results compare favourably with both

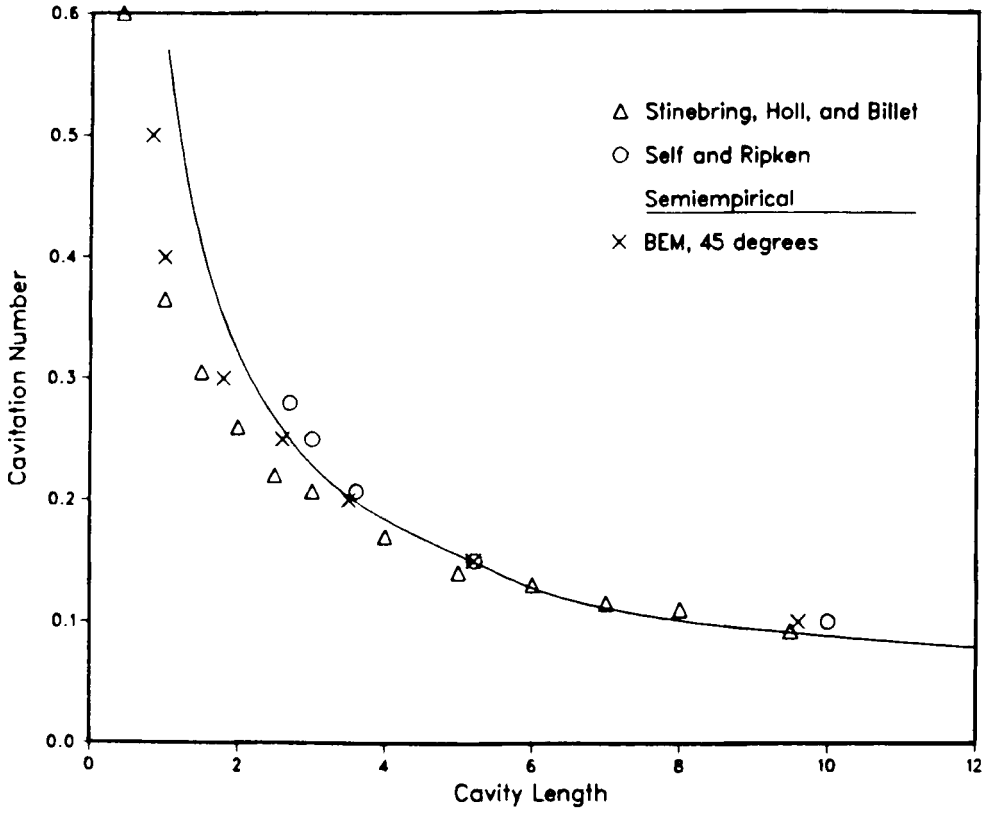

Figure 7. Comparison of DBEM results with water tunnel results of Stinebring *et al.*,[17] water tunnel results of Self and Ripken[23] and Reichardt's[24] semi-empirical formula for relationship between cavitation number and cavity length for 45° conical head

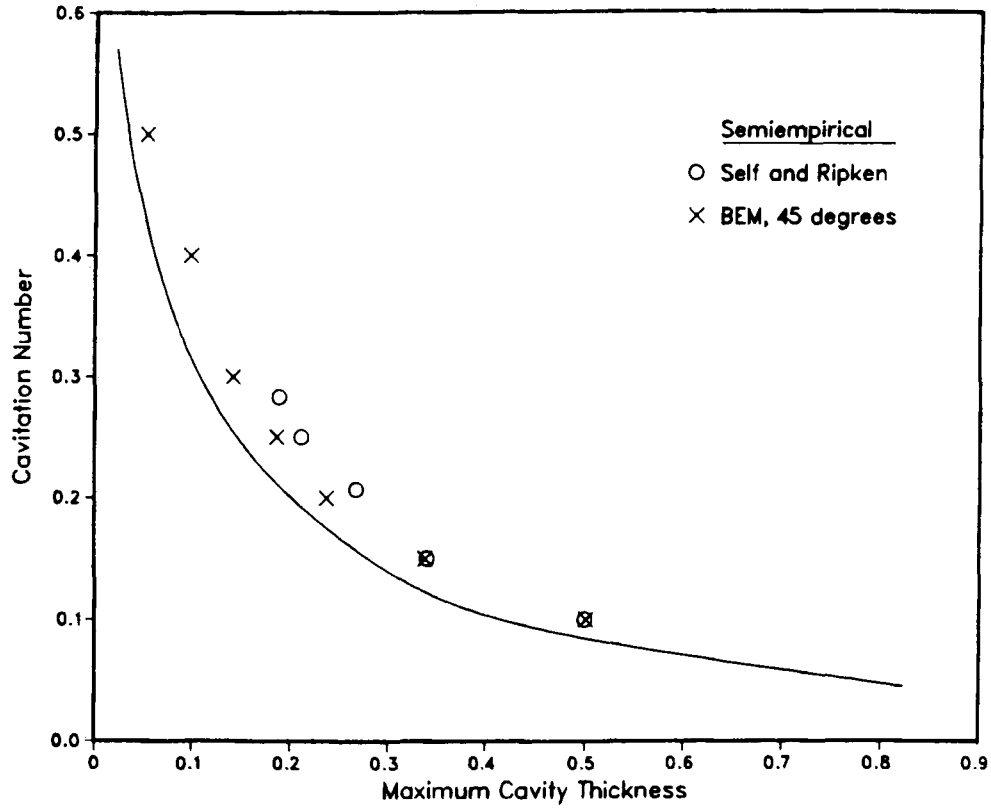

Figure 8. Comparison of DBEM results with water tunnel results of Self and Ripken[23] and Reichardt's[24] semi-empirical formula for relationship between cavitation number and maximum cavity thickness for 45° conical head

Self and Ripken's experimental results and Reichardt's semi-empirical formula. The cavity thickness is seen to increase with decreasing cavitation number and increasing cavity length.

To better demonstrate the mechanics of determining the proper cavity length based on the closure model, we again consider the body comprised of a 45° conical nose and a cylindrical midbody at a cavitation number $K = 0{\cdot}25$. According to our closure model, the slope of the cavity, S, at the body juncture between the nose and midbody should be given by $S = \tan(22{\cdot}5°) = 0{\cdot}414$. For an assumed cavity length the slope of the leading edge of the cavity is approximated from the radius at the body juncture and the radii determined by the inner iteration at the first two body stations under the cavity. Consistent with quadratic representation of the geometry in the DBEM, these three radii together with the quadratic shape functions are used to determine the slope at the leading edge of the cavity. The relationship between the assumed cavity length and the leading edge slope calculated by the DBEM is shown in Figure 9. From this plot the cavity length L as predicted on the basis of our closure model is seen to be given by $L = 2{\cdot}6$. This prediction is substantiated by the water tunnel measurements discussed in the previous paragraph.

RESULTS FOR NON-AXISYMMETRIC FLOWS

The computation of cavity shapes about axisymmetric bodies at an angle of attack involves non-axisymmetric flow fields and is significantly more difficult than for axisymmetric flows. There are

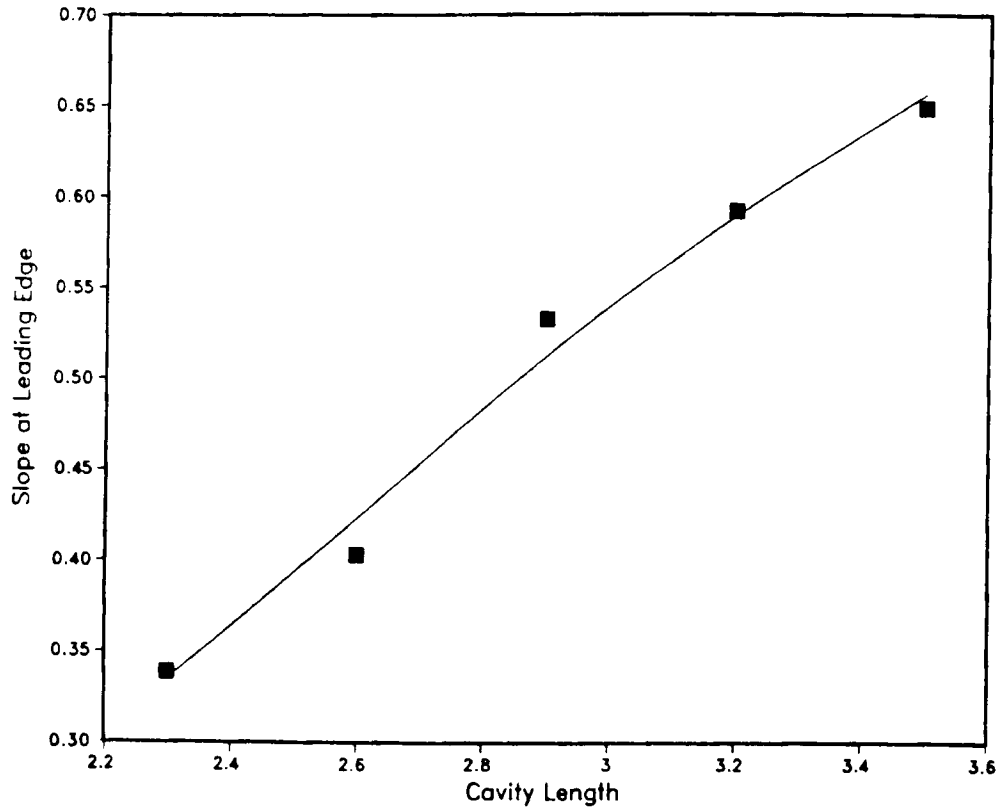

Figure 9. Relationship between assumed cavity length and slope of cavity leading edge for 45° conical head at cavitation number $K = 0{\cdot}25$

several contributing factors for this increase in difficulty besides the increase in the number of parameters necessary to describe the cavity. Both the point of detachment and the cavity length become functions of the polar angle about the axis of symmetry of the body. Nevertheless, the same closure model as discussed above for axisymmetric bodies at zero angle of attack can be extended to axisymmetric bodies at non-zero angle of attack. The extension consists of applying the closure condition along individual longitudinal rays defined by the wetted portion of the body and the cavity at a given polar angle. However, several complications surfaced in our attempt to analyse the non-axisymmetric cavitation problem. The convergence of the inner iteration was much more sensitive to the initial cavity estimate. Further, small errors in specifying the point of detachment resulted in unrealistic converged cavity shapes. These shapes showed oscillations in the cavity thickness at a given body station in the polar direction.

Because of these difficulties, it was necessary to minimize the number of parameters used to describe the cavity. The bodies considered were discretized into 16 longitudinal rays and 19–22 polar rings (Figure 10). Along each ray the thickness of the cavity is specified at three evenly spaced body stations and the shape of the cavity between the body stations is determined by an interpolation scheme. The free stream velocity was oriented in the plane defined by rays 1 and 9 so that, for example, the radii describing the cavity along ray 2 would be identical to the radii along ray 16. Hence the cavity was approximated using a total of 27 parameters. For the bodies

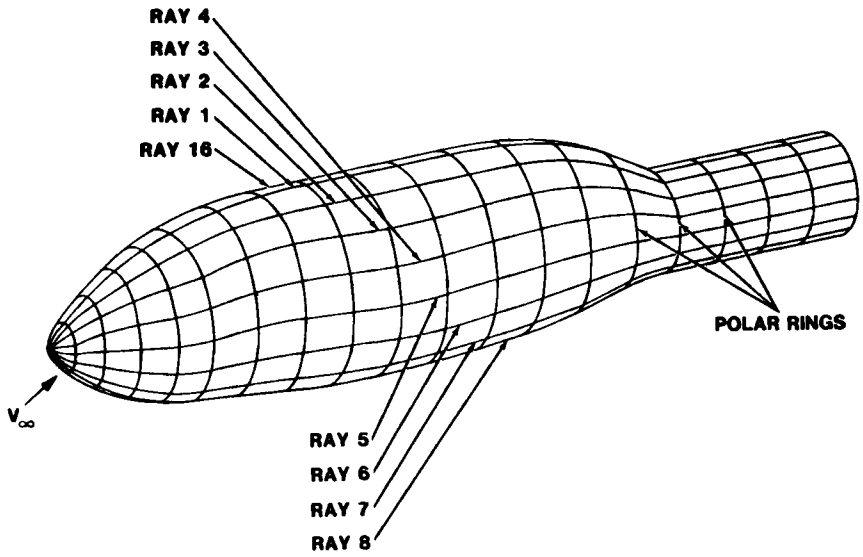

Figure 10. Typical boundary element discretization for symmetric body at angle of attack

considered, the initial cavity shapes were estimated in a similar fashion as for the axisymmetric flows. That is, along a given ray the point of detachment and cavity length were specified. Then the initial cavity shape along that ray was approximated by an arc of a circle which was tangent to the body at the point of detachment and had the prescribed length. In the outer iteration the lengths of the cavity along each ray were adjusted until the converged shape was tangent to the body at each point of detachment along the 16 rays.

The first example of a non-axisymmetric cavity is given by the body comprised of a 45° conical nose and a cylindrical midbody at 6° angle of attack with the cavitation number given by $K = 0{\cdot}4$. This example was chosen since the results could be compared with the water tunnel data of Rouse.[25] Because of the discontinuous body slope, the points of detachment were located at the juncture between the nose and midbody. A comparison between the current DBEM results and the water tunnel data for the coefficient of pressure along the leeward and windward sides of the body is shown in Figure 11. The positive body stations are positioned on the leeward side of the body while the negative body stations are positioned on the windward side of the body. As mentioned above, the length of the cavity along each ray was adjusted until the separating streamline left tangentially to the body. It is seen in Figure 11 that the cavity length on the leeward side is longer than on the windward side. Further, the pressure is seen to be higher on the windward side of the conical nose. The experimental and numerical cavity lengths and pressures agree reasonably well between the water tunnel data and the DBEM results.

The second example of a non-axisymmetric cavity is for a 1·5 calibre ogive body at 3° angle of attack with the cavitation number given by $K = 0{\cdot}24$. This example was more difficult to compute than the first example because the separation zone is three-dimensional. That is, the points of detachment are a function of the polar angle. As mentioned above, perturbations in the location of the points of detachment could result in converged solutions with oscillations in the cavity thickness in the polar direction. It was therefore necessary to refine the grid in the vicinity of the separation region. The cavity shape on the leeward and windward sides of the ogive body is shown in Figure 12. Again the cavity length and thickness are larger on the leeward side of the

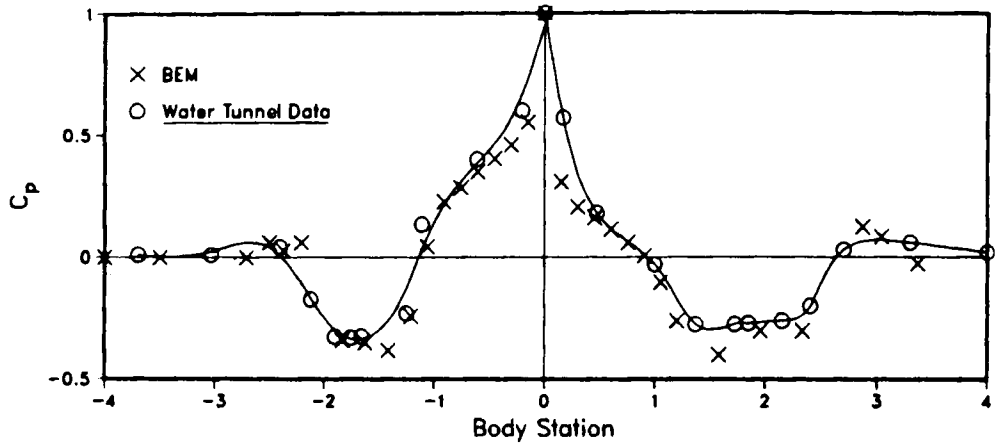

Figure 11. Comparison of DBEM results with water tunnel results of Rouse[25] for coefficient of pressure on body comprised of 45° conical head and cylindrical midbody at 6° angle of attack

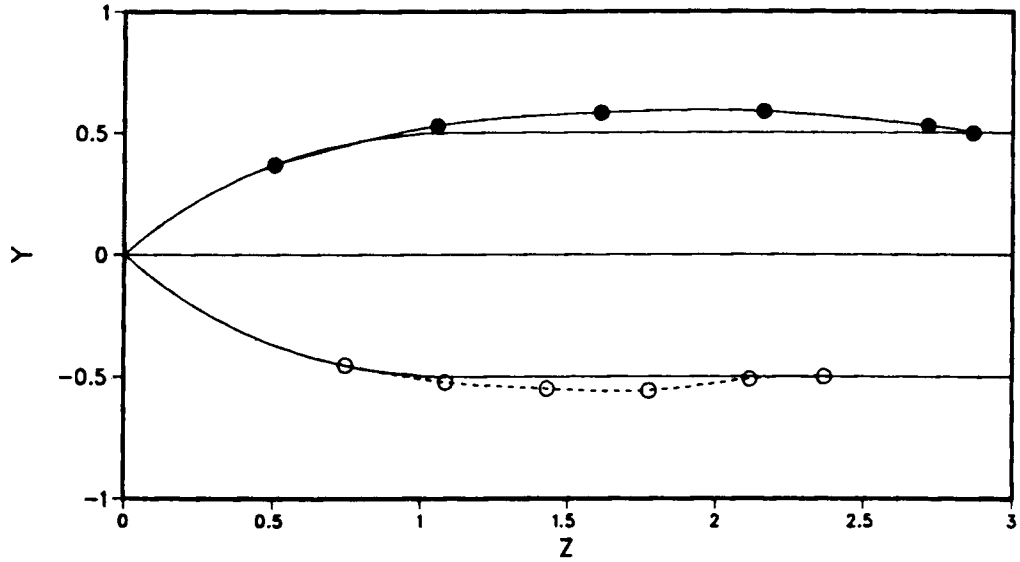

Figure 12. Cavity shape on leeward (top) and windward (bottom) sides of 1·5 calibre ogive body at 3° angle of attack

body as compared to the windward side. Further, the point of detachment on the leeward side is ahead of the point of detachment on the windward side. A plot of the maximum cavity thickness as a function of the polar angle is shown in Figure 13. It is seen in the figure that the cavity thickness increases monitonically as the polar angle increases from the windward (180°) to the leeward (0°) side of the body. A plot of the coefficient of pressure along the leeward and windward sides of the ogive body is shown in Figure 14. It is qualitatively similar to the plot shown in Figure 11 for the body comprised of the conical nose and cylindrical midbody.

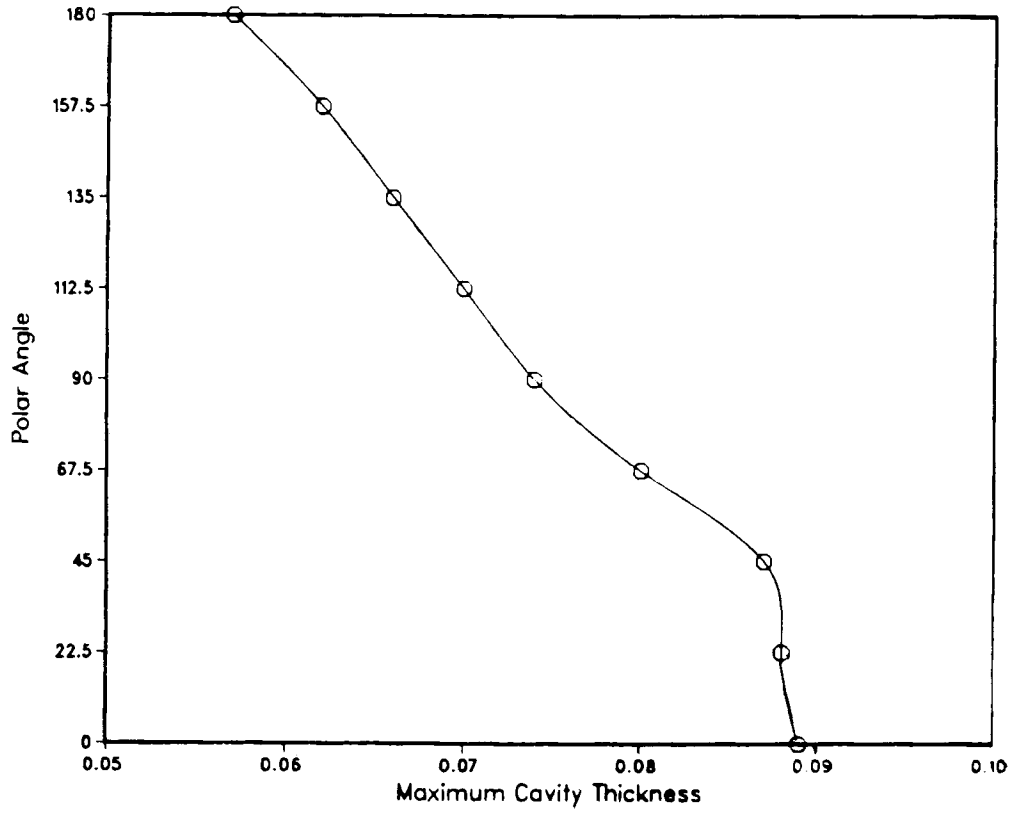

Figure 13. Maximum cavity thickness as a function of polar angle on 1·5 calibre ogive body at 3° angle of attack

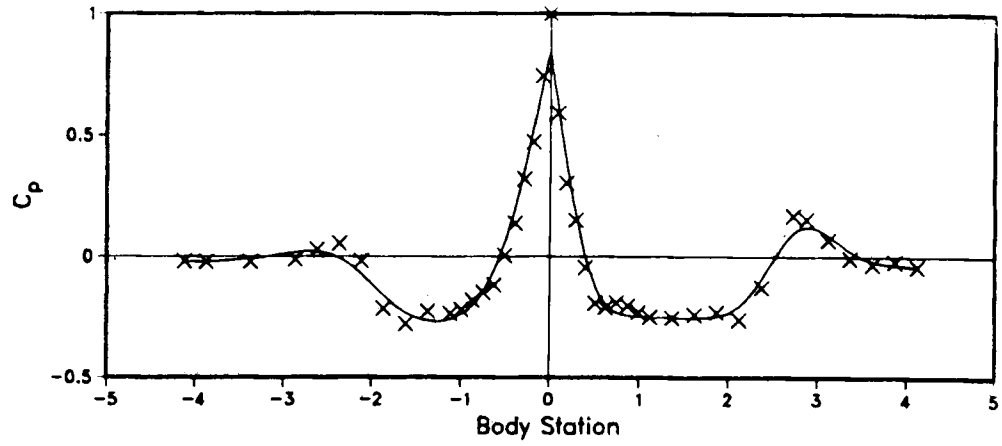

Figure 14. Coefficient of pressure along leeward and windward sides of 1·5 calibre ogive body at 3° angle of attack

CALCULATION OF DRAG ON SUPERCAVITATING CONES

In this section, drag calculations for a family of cones at zero angle of attack are compared with other theory and experiment. The cones are supercavitating, with the cavity leading edge fixed to the base of the cone. We use the closure model discussed previously to determine the cavity length, i.e. the cavity length is varied until the dividing streamline leaves the cone at the cone angle. A graduated mesh is used with the fineness concentrated near the cone/cavity juncture.

The calculated drag force is composed of three values: one due to the pressure distribution over the body, one due to the laminar and/or turbulent skin friction and one due to the base pressure. The axisymmetry of the flow field is used to simplify the force integration. The drag coefficient due to pressure on the lateral surface is given by

$$C_{D_p} = \frac{2\pi}{A_b} \int_0^l C_p r \frac{dr}{dx} dx, \tag{11}$$

where l is the length of the cone, A_b is the area of the base and C_p is the coefficient of pressure found from the DBEM solution. In general, the base drag coefficient is given by

$$C_{D_b} = \frac{p_\infty - p_b}{q} = K, \tag{12}$$

where p_b is the base pressure and q is the dynamic pressure. That is, the base drag pressure is simply the cavitation number. The skin friction drag coefficient is given by

$$C_{D_v} = \frac{2\pi}{q A_b} \int_0^l r\tau dx, \tag{13}$$

where τ is the shear stress on the lateral surface of the cone.

The shear stress distribution is found using a momentum integral boundary layer solution identical to the one described in Reference 22. Both laminar and turbulent boundary layer solutions are found with this scheme. The skin friction drag component can make an important contribution to the total drag. For example, Wolfe *et al.*[22] found that for a 10° cone with a small cavitation number the laminar skin friction drag component represented 44% of the total drag. For 30° cones they found that the skin friction drag represented no more than 6% of the total drag. We show similar results. For the 30° and 45° cone results presented in this section, the skin friction drag contribution is small compared to the pressure drag and base drag contributions. However, we include the viscous effects for completeness.

Drag predictions for 30° and 45° cones for various cavitation numbers are shown in Figure 15. The free stream velocity is assumed to be 20 ft s^{-1}, which is a reasonable value for a water tunnel. The Reynolds number based on length for these calculations is $5{\cdot}1 \times 10^6$ for the 30° cone and $3{\cdot}3 \times 10^6$ for the 45° cone, which results in a laminar boundary layer on both cones. Also plotted in the figure are experimental results of Cox and Maccoll[26] and O'Neill[18] for 30° cones. Theoretical predictions due to Plesset and Schaffer[27] are also shown in the figure. The DBEM predictions show better agreement with experiment for the 30° cone than the predictions of Plesset and Schaffer. This is not surprising since Plesset and Schaffer extended their results for two-dimensional wedges to the case of axisymmetric cones.

Pressure distribution over a 30° cone are shown in Figure 16 for $K = 0{\cdot}05$. The first curve is the DBEM prediction; the second curve is a prediction using the scheme outlined by Wolfe *et al.*[22] Both curves show similar behaviour. The pressure coefficient decreases monotonically from the tip of the cone until the cavitation number is reached at the base of the cone. The solution of Wolfe *et al.* is found using an axial distribution of sources and sinks which limits the solution to

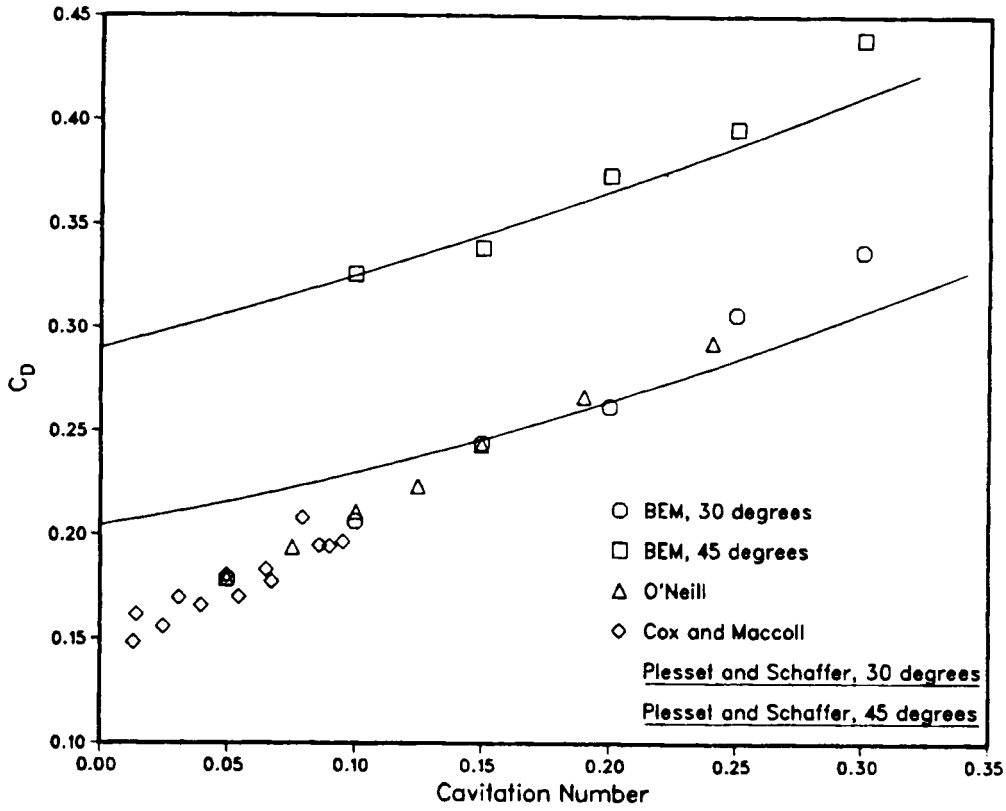

Figure 15. Comparison of DBEM results with water tunnel results of Cox and Maccoll[26] and O'Neill[18] and theoretical predictions of Plesset and Schaffer[27] for drag on 30° and 45° cones

axisymmetric flows. Further, because of numerical ill-conditioning, the scheme due to Wolfe *et al.* is limited to slender bodies.

The influence of the assumed cavity length (the outer iteration parameter) on the drag calculation is shown in Figure 17. Drag coefficients are determined for a 30° cone at a cavitation number $K=0{\cdot}15$ for various assumed cavity lengths. In all cases the pressure along the supercavity has converged to the prescribed cavitation number except at the leading edge of the cavity. The cavity with a length of 3·375 diameters results in the correct drag when compared with experiment. This is also the length that satisfies our closure model. That is, the supercavity leaves the cone at the cone angle with a length of 3·375 diameters. For shorter assumed cavity lengths the supercavity leaves the cone at an angle less than the cone angle and the calculated drag is lower than the experimental values. For longer assumed cavity lengths the supercavity leaves the cone at an angle greater than the cone angle and the calculated drag is higher than the experimental values.

DISCUSSION

A numerical method based on the boundary element method for calculating cavity shapes on axisymmetric bodies at zero and non-zero angles of attack has been developed. In order to

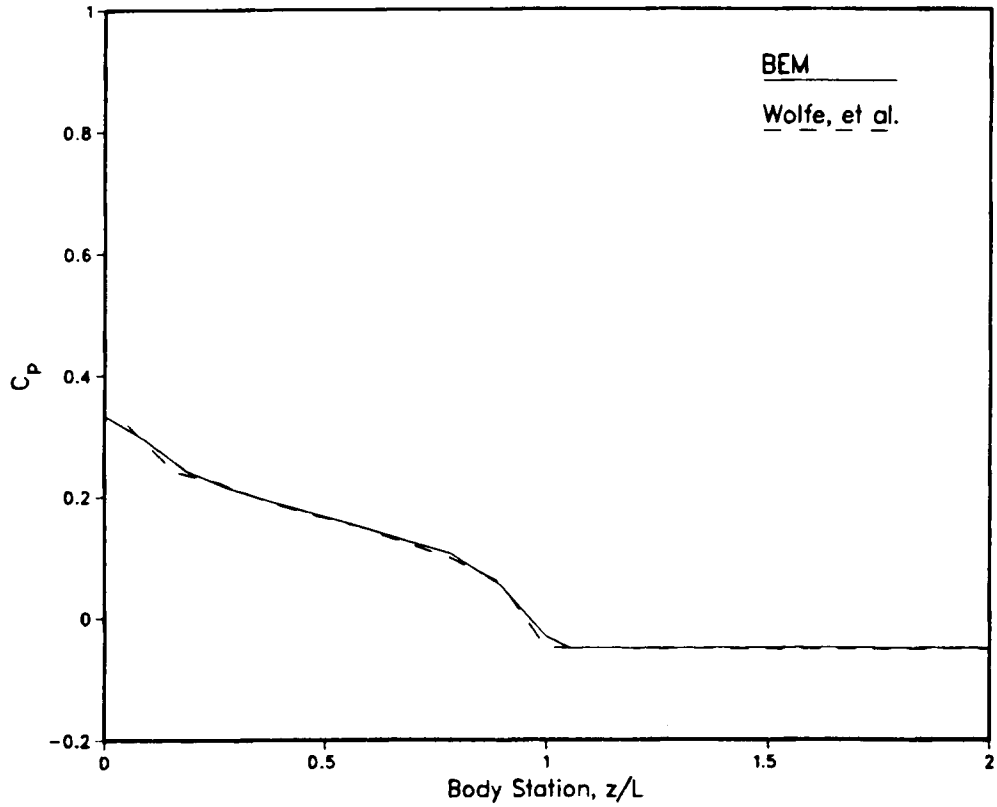

Figure 16. Pressure distribution on supercavitating 30° cone at cavitation number $K = 0{\cdot}05$

properly model the cavity, it is necessary to be able to estimate the cavity length. This problem has been directly addressed with the development of a new closure model that relates the point of detachment, the angle that the separating streamline makes with the body and the cavity length. The closure model has been incorporated into a numerical algorithm based on the direct boundary element method. The model has been extensively tested by comparisons of the numerical predictions with water tunnel measurements. Calculations for both symmetric and non-symmetric flow fields have been performed.

The non-symmetric three-dimensional problem is significantly more difficult computationally because of the sensitivity of the cavity shape to small perturbations of cavity length in a given direction. In fact, in many cases the inner iteration to determine a constant pressure streamline failed to converge because the initial estimate of the cavity shape was inadequate. The sensitivity of the converged solution to the three-dimensional detachment and reattachment zones underscores the importance of being able to accurately determine the extent of the cavity for non-axisymmetric flows. The three-dimensional results presented in this paper are limited. We have only considered axisymmetric bodies at small angles of attack. For larger angles of attack, where separation occurs, our models will certainly break down. Further, modelling of complex three-dimensional bodies such as bodies with tip vortices is still beyond our capabilities.

We have limited our attention in this investigation to relatively slender bodies for which the smooth separation condition can be assumed. However, we feel that our closure model can

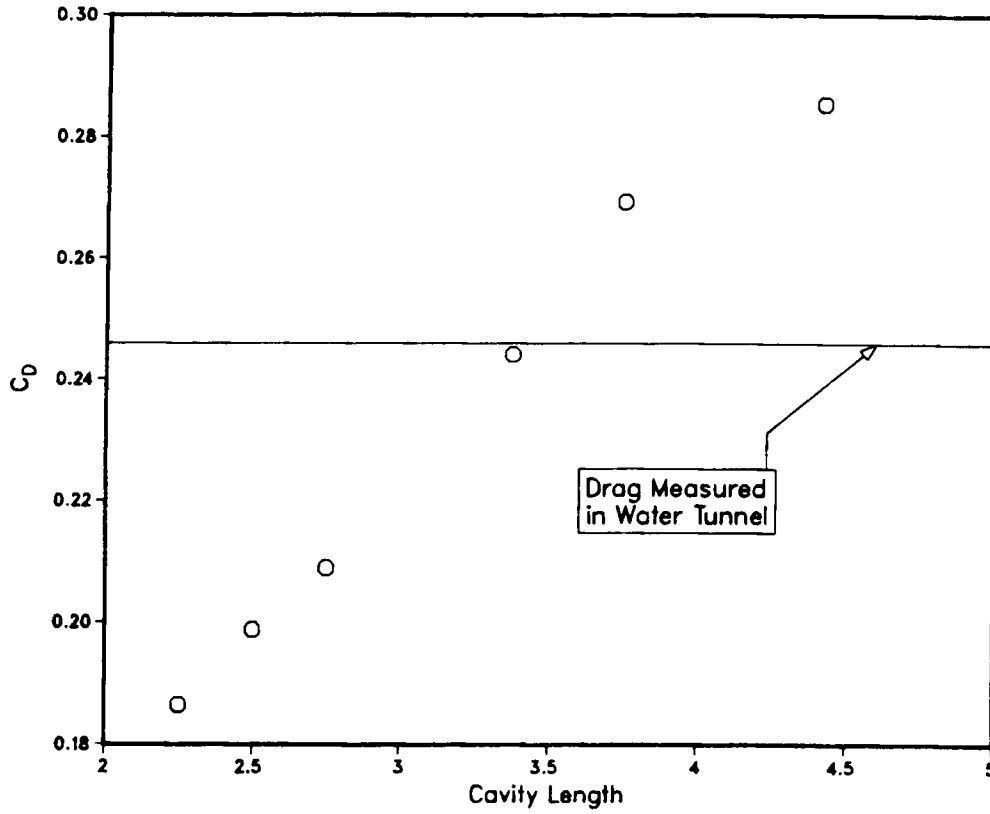

Figure 17. Relationship between assumed cavity length and drag on 30° cone at cavitation number $K = 0{\cdot}15$

possibly be extended to viscous laminar separation for which the smooth separation condition has been shown to be violated. From water tunnel photographs of viscous laminar separation it appears that the dividing streamline leaves the body at an oblique angle just downstream of the laminar separation bubble. By incorporating information from water tunnel experiments and information obtained from numerical simulations of laminar separation, it may be possible to determine empirical expressions for the position of the leading edge of the cavity and the angle that the dividing streamline makes with the body that can be incorporated into the current closure model, which will again allow for accurate modelling of the cavity.

ACKNOWLEDGEMENTS

This work was supported by Sandia National Laboratories and the U.S. Department of Energy under contract DE-AC04-76DP00789. The original negatives from the Rouse and McNown experiments were graciously lent to us by the University of Iowa.

REFERENCES

1. M. S. Plesset, 'The dynamics of cavitation bubbles', *J. Appl. Mech. ASME*, **16**, 277–282 (1949).
2. V. H. Arakeri, 'Viscous effects on the position of cavitation separation from smooth bodies', *J. Fluid Mech.*, **68**, 779–799 (1975).

3. D. Riabouchinski, 'On steady fluid motion with free surfaces', *Proc. Lond. Math. Soc.*, **19,** 206–215 (1920).
4. N. E. Joukowsky, 'I. A modification of Kirchoff's method of determining a two-dimensional motion of a fluid given a constant velocity along an unknown streamline. II. Determination of the motion of a fluid for any condition given on a streamline', *Rec. Math.*, **25,** 121–278 (1890).
5. T. Y. Wu, 'A wake model for free-streamline flow theory: Part 1, Fully and partially developed wake flows and cavity flows past an oblique flat plate', *J. Fluid Mech.*, **13,** 161–181 (1962).
6. G. Kreisel, 'Cavitation with finite cavitation numbers', *Admiralty Res. Lab. Rep. r1/h/36*, 1946.
7. M. P. Tulin, 'Supercavitating flows—small perturbation theory', *J. Ship Res.*, **7,** (3), 16–37 (1964).
8. H. Lemonnier and A. Rowe, 'Another approach in modelling cavitating flows', *J. Fluid Mech.*, **195,** 557–580 (1988).
9. M. Brillouin, *Ann. Chim. Phys.*, **23,** 145–230 (1911).
10. H. Villat, 'Sur la validité des solutions de certains problèmes d'hydrodynamique', *J. Math.*, **10,** (6), 231–290 (1914).
11. C. Brennen, 'A numerical solution of axisymmetric cavity flows', *J. Fluid Mech.*, **37,** 671–688 (1969).
12. T. R. Mogel and R. L. Street, 'A numerical method for steady state cavity flows', *J. Ship Res.*, **18,** (1), 22–31 (1974).
13. O. Furuya, 'Nonlinear calculation of arbitrary shaped supercavitating hydrofoils near a free surface', *J. Fluid Mech.*, **68,** 21–40 (1975).
14. C. Pellone and A. Rowe, 'Supercavitating hydrofoils in non-linear theory', in J. C. Dern and H. J. Haussling (eds), *Proc. Third Int. Conf. on Numerical Ship Hydrodynamics*, Paris, June 1981, Bassin d'Essais des Carènes, Paris, 1981, pp. 399–412.
15. A. Dagan, 'Axially symmetric cavitation flow at small cavitation numbers', *Int. j. numer. methods fluids*, **8,** 943–955 (1988).
16. J. M. Aitchison and A. Karageorghis, 'Numerical solution of a free surface problem by a boundary element method', *Int. j. numer. methods eng.*, **8,** 91–96 (1988).
17. D. R. Stinebring, J. W. Holl and M. L. Billet, 'Water tunnel investigation of ventilated cavities on conical head bodies—Part 2', in J. H. Kim, O. Furuya and B. R. Parkin (eds), *Jets and Cavities—Int. Symp., ASME FED*, Vol. 31, ASME, New York, 1985, pp. 203–214.
18. J. P. O'Neill, 'Flow around bodies with attached open cavities', *California Institute of Technology Hydrodynamics Laboratory Report E-24.7*, 1954.
19. H. Rouse and J. S. McNown, 'Cavitation and pressure distribution. Head forms at zero angle of yaw', *State University of Iowa, Eng. Bull. 32*, 1948.
20. C. A. Brebbia, J. C. F. Telles and L. C. Wrobel, *Boundary Element Techniques*, Springer, Berlin, 1984.
21. A. K. Mitra and M. S. Ingber, 'Resolving difficulties in the BIEM caused by geometric corners and discontinuous boundary conditions', in C. A. Brebbia, W. L. Wendland and G. Kuhn (eds), *Boundary Elements IX*, Stuttgart, September 1987, Springer, Berlin, 1987, pp. 519–534.
22. W. P. Wolfe, C. E. Hailey and W. L. Oberkampf, 'Drag of bodies of revolution in supercavitating flow', *J. Fluids Eng.*, **111,** 300–305 (1989).
23. M. W. Self and J. F. Ripken, 'Steady-state cavities studies in a free-jet water tunnel', *SAF Project Rep. 47*, 1955.
24. H. Reichardt, 'The laws of cavitation bubbles at axially symmetric bodies in a flow', *MAP Rep. Transl. 766*, 1946.
25. H. Rouse, 'Cavitation and pressure distribution. Head forms at angles of yaw', *State University of Iowa, Eng. Bull. 42*, 1962.
26. R. N. Cox and J. W. Maccoll, 'Recent contributions to basic hydroballistics', *Naval Symp.* 1957, pp. 215–239.
27. M. S. Plesset and P. A. Schaffer, 'Cavity drag in two and three dimensions', *J. Appl. Phys.*, **19,** 934–939 (1948).